J. Fluid Mech. (1974), *vol.* 65, *part* 1, *pp.* 97–112
Printed in Great Britain

Measurements of velocity distributions in the wake of a circular cylinder at low Reynolds numbers

By MICHIO NISHIOKA
College of Engineering, University of Osaka Prefecture, Japan
AND HIROSHI SATO
Institute of Space and Aeronautical Science, University of Tokyo, Japan

(Received 29 October 1973)

Velocity measurements were made in the flow field behind a circular cylinder at Reynolds numbers from 10 to 80 and results compared with existing numerical solutions. Takami & Keller's solution for the velocity distribution in the wake shows good agreement at low Reynolds numbers and fair agreement at high Reynolds numbers. The drag coefficient of the cylinder and the size of the standing eddies behind the cylinder were also determined. They are compatible with existing experimental and numerical results. Details of the velocity distribution in the standing eddies are clarified.

1. Introduction

For two-dimensional steady flow past a circular cylinder at low Reynolds number experimental data are available on the pressure distribution on the cylinder surface (Thom 1933; Grove *et al.* 1964; Acrivos *et al.* 1965, 1968), the drag coefficient (Tritton 1959) and the flow pattern including eddies behind the cylinder (Taneda 1956; Acrivos *et al.* 1965, 1968). However, there are not many measurements of the velocity distribution in the wake except those by Kovasznay (1949) and Grove *et al.* (1964).

Numerical solutions of the Navier–Stokes equation for the flow around a cylinder have been obtained by several authors: at $R = 10$ and 20 by Thom (1933), at $R = 40$ by Kawaguti (1953) and at $R = 40$ and 44 by Apelt (1961). Recently, using a method similar to that of Kawaguti (1953), Keller & Takami (1966) obtained solutions for $R = 2$–15. Subsequently, the Reynolds number range of the solution was extended up to 60 by Takami & Keller (1969) and to 100 by Dennis & Chang (1970). These solutions were compared with experimental results for the pressure distribution, the drag coefficient and the size of standing eddies behind the cylinder and mostly good agreement was demonstrated. However, these solutions give quite different results for the velocity distribution in the wake.

The purpose of the present study was to make detailed measurements in the wake of a cylinder and compare the data with existing numerical results. A systematic wind-tunnel experiment was carried out to find the velocity distribution at Reynolds numbers based on the cylinder diameter ranging from

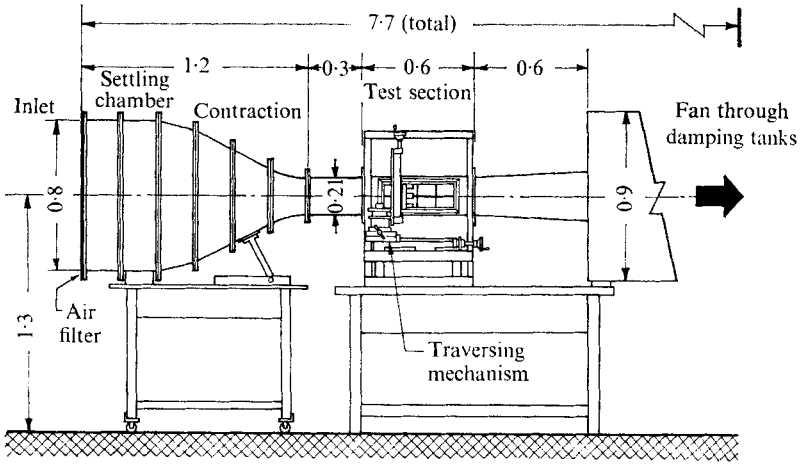

FIGURE 1. Low-turbulence low-speed wind tunnel; scale in metres.

10 to 80. In particular, velocity distributions inside the standing eddies were measured in detail at $R = 65$ and 80. Only some of experimental results are presented here. The entire set of data may be found in Nishioka (1972).

2. Apparatus and preliminary tests

2.1. *Wind tunnel*

The measurements were made in a suction-type wind tunnel whose test section is 20×20 cm in cross-section and 60 cm long, as shown in figure 1. An electric fan for domestic use is installed to generate the flow. The wind speed in the test section may be varied from 3 cm/s to 150 cm/s by adjusting the voltage of a stabilized a.c. supply. An air filter made of cotton and flannel cloths is stretched across the inlet, which is 80×80 cm in cross-section, and five fine-mesh damping screens span the settling chamber. The contraction ratio is 16. Two damping tanks ($90 \times 90 \times 180$ cm and $50 \times 50 \times 170$ cm) are installed between the test section and the fan to prevent the fan noise from reaching the test section as well as to reduce the fluctuations in the test section due to changes in atmospheric conditions.

This arrangement provides a uniform flow in the test section with a velocity variation of less than 1% over the region of the wake survey and less than 2% over the entire cross-section excluding the wall boundary layer. The free-stream turbulence is about 0·1%. Measurements were made only when the room temperature was steady, because the heat loss rate from a hot-wire anemometer at an extremely low wind speed is affected seriously by temperature variations in the laboratory.

One of the side walls of the test section contains slits in the horizontal and vertical directions, and a hot-wire probe mounted on a three-dimensional traversing mechanism is inserted into the test-section through one of these slits. Leakage of air through these slits is carefully prevented.

R	10	15	20	30	40		50		55	60		65	75	80
d (mm)	2·01	2·01	2·01	4·03	4·03		2·01	4·03	4·03	2·01	4·03	4·03	4·03	4·03
L/d	100	100	100	50	50	6·5	100	6·5	6·5	100	6·5	6·5	6·5	6·5
U_∞ (cm/s)	8·1	11·8	14·9	11·3	15·1	15·6	37·3	19·5	21·1	44·8	23·1	25·0	28·9	30·8

TABLE 1. Experimental conditions

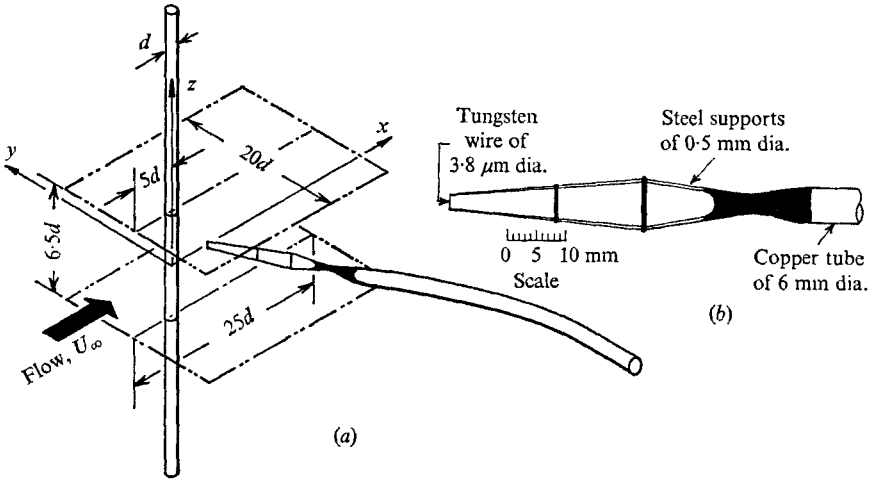

FIGURE 2. (*a*) Arrangement of cylinder and hot-wire probe in test section. The 4 mm cylinder with end-plates (dot–dashed lines) is shown. d denotes the diameter of the cylinder. (*b*) Details of hot-wire probe. ■, araldite.

2.2. *Circular cylinder*

Two circular cylinders were used for the experiment. They are 2·01 mm and 4·03 mm in diameter and are referred to as the 2 mm cylinder and 4 mm cylinder, respectively. These cylinders are made of bakelite, whose low heat conductivity reduces the effect of the wall on the heat loss from the hot-wire anemometer. The range of Reynolds numbers obtained using these cylinders is shown in table 1 together with other experimental conditions. Each cylinder spanned the test section vertically in the centre-plane as shown in figure 2(*a*). The z axis coincides with the axis of the cylinder, the x axis is in the direction of the undisturbed flow (horizontal) and the y axis is perpendicular to the other two.

The length-to-diameter ratio of the cylinder is a very important factor in the development of the wake at Reynolds numbers from 40 to 150. The critical Reynolds number for vortex shedding from the cylinder depends strongly on this ratio. Figure 3 shows the critical Reynolds number plotted against the length-to-diameter ratio. If the ratio is large enough vortex shedding takes place at around $R = 40$. As the ratio is decreased the critical Reynolds number increases. Measurements indicate that the vortex street formed behind the cylinder has a spanwise wavelength of 15–20 diameters. This suggests that the vortex shedding does not occur two-dimensionally at large length-to-diameter ratios. As the ratio is decreased the standing vortex behind the cylinder is

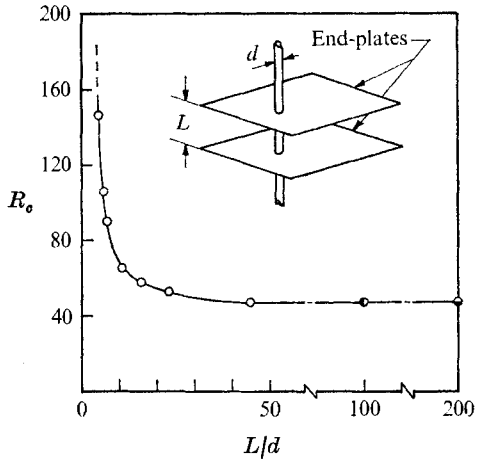

FIGURE 3. Effect of length-to-diameter ratio of cylinder on the critical Reynolds number for vortex shedding. ○, d = 4 mm; ◐, d = 2 mm; ◒, d = 1 mm.

stabilized and vortex shedding does not take place until larger Reynolds numbers. For the present experiment we have used the ratio 6·5 for experiments at high Reynolds numbers. In this case the critical Reynolds number for vortex shedding is about 85, and the length of the flat portion of the z-wise velocity distribution in the wake of the 4 mm cylinder at $y/d = -3$ and $x/d = 20$ is at least $1{\cdot}4d$, $1{\cdot}8d$ and $2{\cdot}1d$ at $R = 40$, 65 and 80, respectively.

2.3. *Calibration of hot-wire anemometer and linearizer for use at extremely low wind speeds*

A hot-wire anemometer is the most suitable instrument for the present experiment because of the small size of the sensing element and the higher sensitivity at low wind speeds. King's law and the empirical relation of Collis & Williams (1959) provide a basis for the prediction of the forced-convection heat transfer from a hot wire. Neither of them is, however, applicable to a hot wire working at wind speeds below 100 cm/s, because the amount of heat lost owing to forced convection is much smaller than losses due to the free convection and the conduction from the support of the wire. Therefore, as the first step in the experiment the rate of heat loss from the wire was examined for various values of the length-to-diameter ratio $(l/d)_w$ of the wire and the wire overheat ratio and different wire orientations relative to the direction of gravity. The hot wires consist of tungsten wire 3·8 μm in diameter and 1 mm and 2·5 mm in length. Details of the probe are shown in figure 2 (*b*).

The heat loss for an overheat ratio of 0·6 is shown in figure 4 and effects of $(l/d)_w$ and the wire orientation are illustrated. The ordinate Nu denotes the non-dimensional average heat loss rate per unit length, and U the wind speed. The heat loss rate was measured with a low-noise constant-temperature anemometer system (Nishioka & Sato 1970) and the wind speed was determined by the method explained in the next section. It is first noted that the relation between

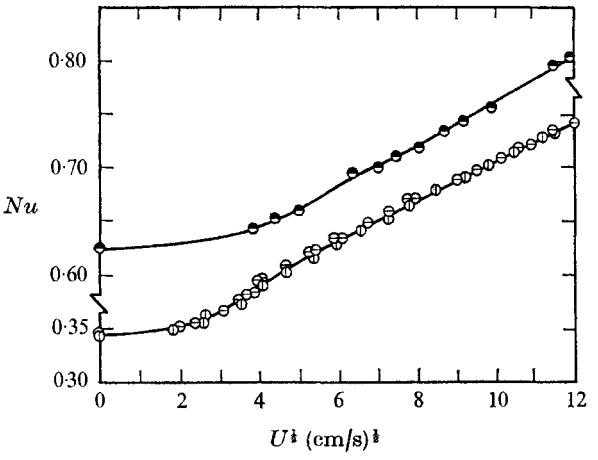

FIGURE 4. Heat loss relations at extremely low wind speeds for an overheat ratio of 0·6. ●, $(l/d)_w = 260$, horizontal wire; ⊖, $(l/d)_w = 650$, horizontal wire; ⊙, $(l/d)_w = 650$, vertical wire.

Nu and $U^{\frac{1}{2}}$ is linear at wind speeds higher than a certain value irrespective of the wire orientation and of $(l/d)_w$. At wind speeds below a critical value the relation is no longer linear but resembles the shape of a spoon. The critical wind speed is higher for smaller $(l/d)_w$ and in this example it is 60 cm/s and 30 cm/s for $(l/d)_w = 260$ and 650, respectively. On the other hand, the wire orientation has little influence on the spoon-shape characteristics. Results of numerous similar measurements with various overheat ratios from 0·15 to 0·8 indicate that the spoon shape becomes slightly flatter as the overheat ratio is increased.

In order to make the calibration curve linear, that is, the output voltage proportional to the wind speed, a linearizer for use at wind speeds from 0 to 150 cm/s was constructed. It is essentially an arbitrary-function generator which consists of biased PNP and NPN transistors. It is capable of linearizing a function with inflexion points. Kovasznay & Chevray (1969) proposed a method of temperature compensation of a linearizer using germanium transistors. The silicon transistors used for the present linearizer have lower leakage and higher temperature stability and the temperature drift was proved to be extremely small. Details of the linearizer are described elsewhere (Nishioka 1973). All the velocity distribution measurements were made using a constant-temperature anemometer with the linearizer. An example of the calibration curve of the linearized anemometer is shown in figure 5. The linearity is satisfactory.

2.4. *Observation of vortex shedding in connexion with the determination of wind speed*

The wind speed was determined by two methods. One is the so-called heat-wake method, in which a sinusoidal heat wake generated by passing a sinusoidal current through a signalling hot wire is used as a tracer and the wavelength is measured by the second temperature-sensitive hot wire. This is an absolute measurement. In the second method the wind speed is determined by measuring

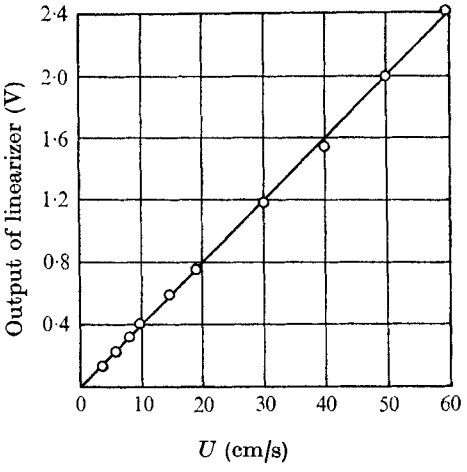

FIGURE 5. Calibration curve of linearized anemometer.

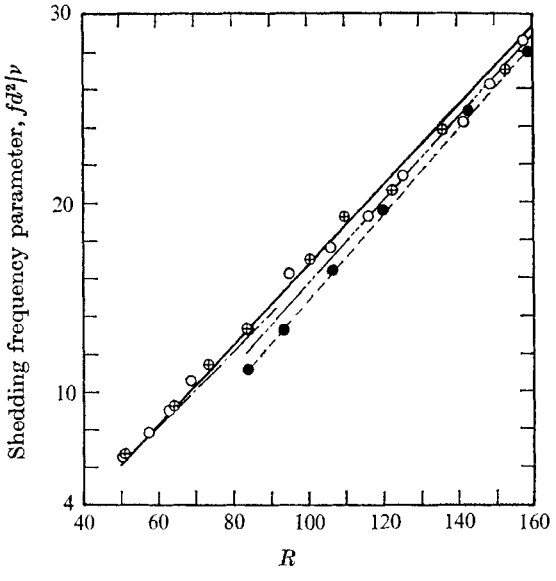

FIGURE 6. Vortex shedding parameter *vs.* Reynolds number. Experimental conditions: ⊕, $d = 4$ mm, $L/d = 50$; ○, $d = 5$ mm, $L/d = 4$; ●, $d = 4$ mm, $L/d = 6{\cdot}5$. ——, Roshko's proposal. Tritton's proposals: — — —, low-speed mode; — — — —, high-speed mode.

the frequency of vortex shedding from a circular cylinder. The relation between R and the shedding parameter fd^2/ν was first examined by observing the shedding frequency f and U_∞ determined by the heat-wake method. This observation was made using long 4 mm and 5 mm cylinders. Instability of the wake begins at around $R = 48$ and regular and stable vortex streets are formed for $R > 50$. The measured relation between fd^2/ν and R is in good agreement with that of Roshko (1954) for $R < 110$ as shown in figure 6. After this result had been

established, the wind-speed measurement for the calibration of the hot-wire anemometer was made by measuring the shedding frequency.

Tritton (1959) found a small discontinuity in the relation between fd^2/ν and R around $R = 90$. He observed a certain kind of irregular vortex shedding and he distinguished two modes of vortex shedding for $R \lesssim 90$, calling them the 'low-speed mode' and 'high-speed mode', respectively. Judging from the present data, there seems to be a similar discontinuity at $R \fallingdotseq 110$ instead of 90. For $R > 110$ the experimental points fall on the line proposed by Tritton for the high-speed mode. However, in contrast to Tritton's observations no irregular vortex shedding is found until R exceeds 180. Because of these ambiguities in the relation between fd^2/ν and R at high Reynolds numbers, we use the relation only for $R < 110$ in determining the wind speed.

2.5. *Problems associated with the measurement of low air speeds*

As a hot wire approaches a solid wall the heat loss rate increases considerably, and as a result the anemometer indicates a large apparent velocity. Because the forced convection is small at low air speeds, the wall effect due to the conduction becomes appreciable when the distance of the wire from the wall is about 2 mm in the case of a metal wall and about 1·5 mm in the case of a bakelite wall. This is the reason why bakelite cylinders were used in the present experiment. After several attempts to correct the reading of the hot wire near the wall we reached the conclusion that the wall effect was too large to be corrected. Therefore, we discarded experimental results at distances within 1 mm from the cylinder.

The possibility that the physical presence of the probe might disturb the flow and so introduce significant errors was investigated (at a Reynolds number of 40) by introducing a second probe at a distance of about one diameter in the z direction. The resulting change in the velocity measurements was negligible and it was concluded that any effect was small compared with the wall effect mentioned above.

Another problem is the spatial resolution of the hot wire. Measurements in very thin wakes indicate that the effective 'diameter' of the hot wire can be as large as 0·2 mm although the physical diameter is only 0·0038 mm. This is due to the large volume of the free convection zone around the hot wire. The resolution of the hot wire at low air speeds is considered to be around 0·2 mm.

3. Results and discussion

3.1. *Velocity distribution downstream of standing eddies*

The velocity distributions were measured at various x/d positions for $R = 10$, 15, 20, 30, 40, 50 and 60 under the experimental conditions shown in table 1. The two-dimensionality of the flow at $R = 10$ is quite good as shown in figure 7. Three distributions about $19d$ apart in the z direction coincide. The anemometer indicates the absolute magnitude of the resultant velocity U. In the wake downstream of standing eddies U is almost equal to the x component. The velocity distributions at $R = 10$ and 40 are shown to illustrate the development of the

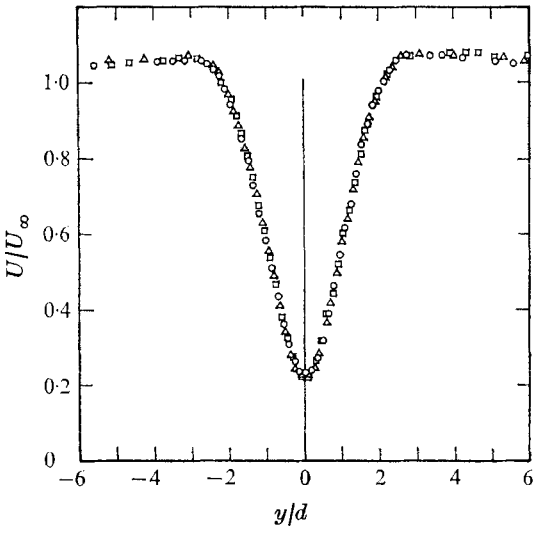

FIGURE 7. Two-dimensionality of wake. Velocity distributions at $x/d = 3{\cdot}0$, $R = 10$: □, $z/d = 8{\cdot}5$; ○, $z/d = 0$; △, $z/d = -10{\cdot}3$.

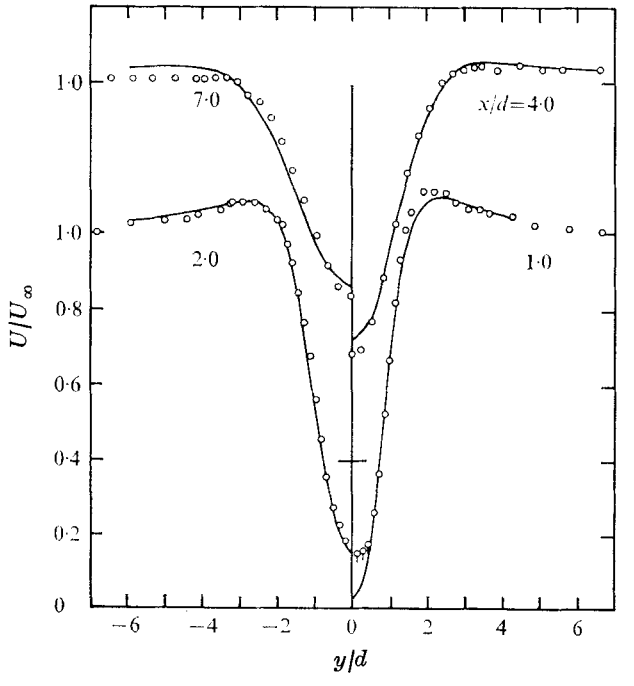

FIGURE 8. Wake velocity distributions at $R = 10$. ○, present measurements ($L/d = 100$); ——, Takami & Keller's numerical solution. A flag on a symbol indicates that the hot-wire reading was affected by the wall.

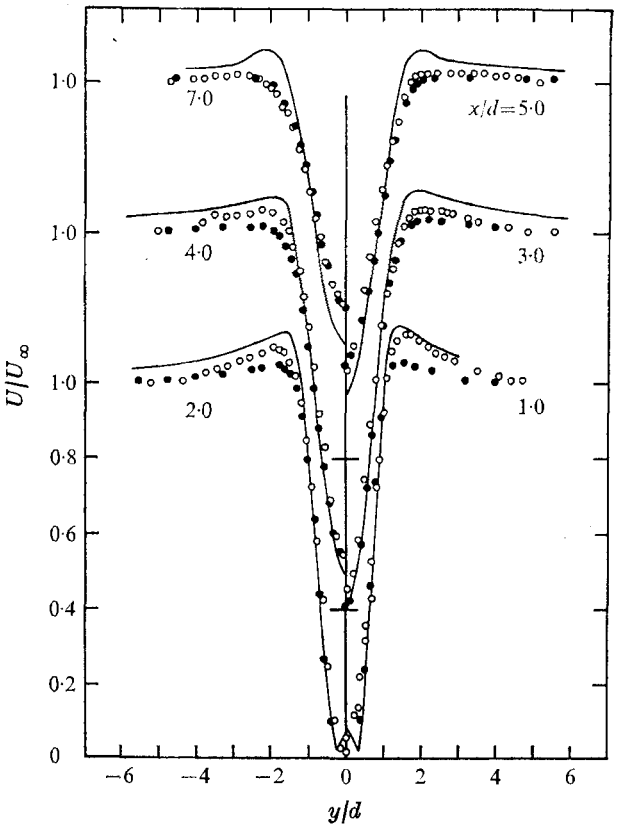

FIGURE 9. Wake velocity distributions at $R = 40$. Present measurements: ○, $L/d = 50$; ●, $L/d = 6·5$. ——, Takami & Keller's numerical solution.

wake in figures 8 and 9. The non-dimensional velocity U_c/U_∞ on the centre-line of the wake is plotted against x/d in figure 10 for $R = 10$, 20 and 40. The numerical solutions of Kawaguti, Apelt and Takami & Keller are shown for comparison. Also included in figure 10 are measurements of Kovasznay ($R = 34$) and the analytical results of Imai (1951) for the far-field wake.

It is observed in figure 8 that the solution of Takami & Keller agrees well with experimental results at $R = 10$. In figure 9, however, there are some discrepancies especially at large y/d. The centre-line velocity in figure 10 shows good agreement with Takami & Keller's results at small x/d for all Reynolds numbers. At large x/d there is a disagreement at $R = 20$. At $R = 40$ Takami & Keller's results do not extend to large x/d. Measurements of Kovasznay and solutions of Kawaguti and Apelt all disagree with the present results. Imai's formula agrees with the experimental data very well for $x/d > 10$.

Non-dimensionalized velocity-defect distributions at various Reynolds numbers are shown in figure 11. The non-dimensional velocity defect

$$(U_\infty - U)/(U_\infty - U_c)$$

is plotted against y/b, where b denotes the half-width of the wake. Distributions for different values of R collapse onto a single curve at $x/d = 10$ as shown in the

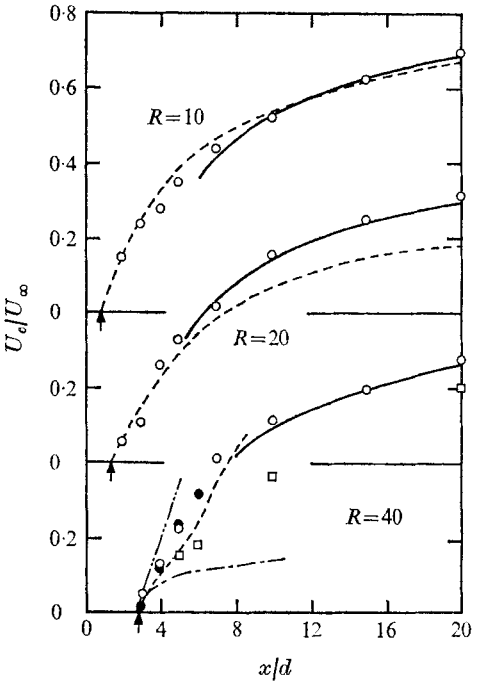

FIGURE 10. Development of velocity along the centre-line of wake. Present measurements: ○, $L/d = 50$; ●, $L/d = 6{\cdot}5$. □, Kovasznay's measurements ($R = 34$); ——, Imai's analytical result. Numerical solutions: – – – –, Takami & Keller; — — —, Apelt, — — — —, Kawaguti. Arrows indicate the wake stagnation point from Takami & Keller's solutions.

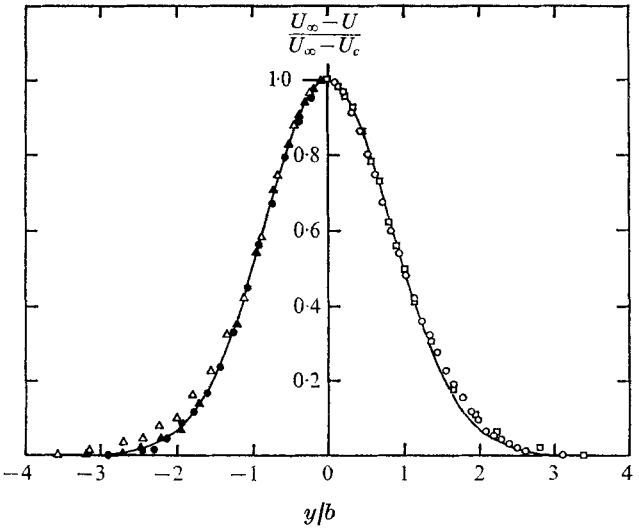

FIGURE 11. Velocity-defect distributions at $x/d = 10$. ——, theoretical, similar distribution; ○, $R = 10$; ●, $R = 15$; △, $R = 20$; ▲, $R = 30$; □, $R = 40$.

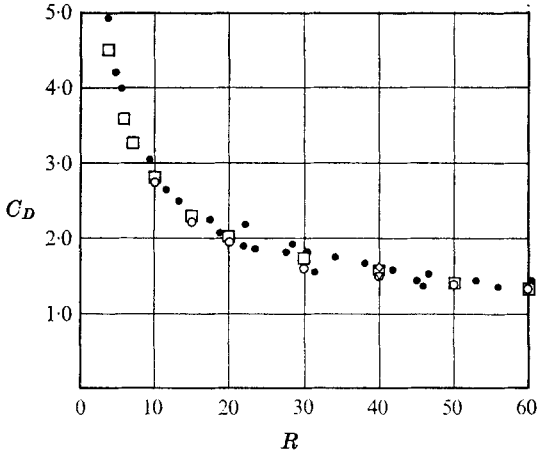

FIGURE 12. Drag coefficient *vs.* Reynolds number. Experimental results: ○, present work; ●, Tritton. Numerical solutions: □, Takami & Keller; ◇, Kawaguti; ▽, Apelt.

figure. The measured distributions are well represented by the following theoretical distribution obtained for the wake by assuming similarity:

$$(U_\infty - U)/(U_\infty - U_c) = \exp\{-0{\cdot}693(y/b)^2\}.$$

This suggests that the static pressure recovers to its undisturbed value at around $x/d = 10$. This can be ascertained also by examining the streamwise development of the momentum thickness θ, defined by

$$\theta = \frac{1}{U_\infty^2}\int_{-\infty}^{\infty} U(U_\infty - U)\,dy.$$

Experimental results indicate that θ first increases with x/d but levels off at around $x/d > 10$. The drag coefficient of the cylinder is given by $2\theta/d$ estimated at large x/d. The drag coefficient determined by this method is plotted against R in figure 12, together with other experimental (Tritton 1959) and numerical results. The present results for $R = 50$ and 60 were obtained from the velocity distributions of unsteady wakes with vortex shedding. Results of numerical solutions of Kawaguti, Apelt and Takami & Keller agree well with Tritton's and the present measurements.

3.2. *Velocity distributions in standing eddies*

Velocity distributions close to the cylinder at $R = 80$ are shown in figure 13. The non-dimensional velocity U_c/U_∞ on the centre-line of the wake is plotted against x/d for $R = 40, 55, 60, 65, 75$ and 80 in figure 14. These measurements were made using the 4 mm cylinder with end-plates and a length-to-diameter ratio of 6·5. In figure 14, at $R = 80$, U_c/U_∞ increases with x/d just behind the cylinder, becomes a maximum (actually a negative maximum), decreases until it reaches a minimum and again increases downstream. This variation suggests the existence of a stagnation point in the wake. On the other hand, as seen in figure 13, distributions at x stations between the cylinder and the stagnation point in the

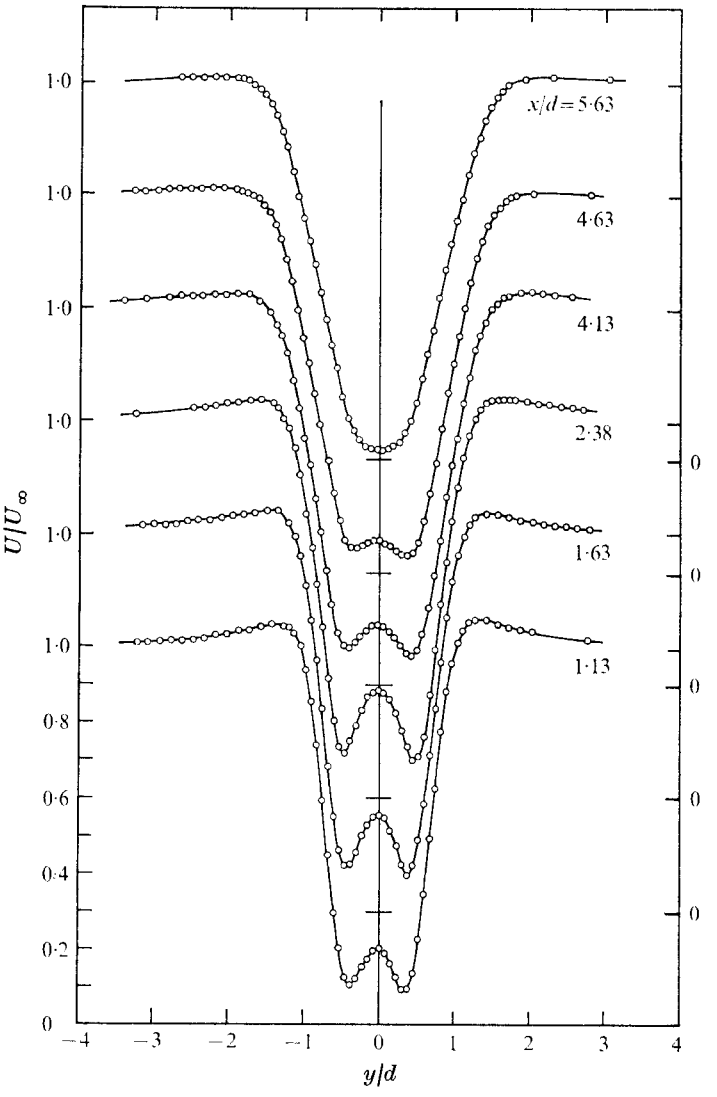

FIGURE 13. Velocity distributions across standing eddies at $R = 80$.

wake have W-shaped portions which suggest reversed flows at small y/d. These facts indicate the existence of closed streamlines at positive and negative y, namely, a pair of standing eddies. Since the W-shaped distributions are almost symmetric with respect to the centre-line of the wake, the standing eddies seem to be symmetric with respect to the centre-line. The centre of the eddy may be determined from velocity distributions. Using data presented in figure 13, the streamwise variations of the velocity along lines of constant y/d are replotted in figure 15. The distributions for $y/d = 0{\cdot}45$, $0{\cdot}525$ and $0{\cdot}6$ have valleys, while those for $y/d = 0$, $0{\cdot}30$ and $0{\cdot}375$ have peaks. The velocity must be zero at the centre of the eddy if it exists. Owing to the slight oscillation of the eddy centre and owing also to the limited spatial resolution of the hot wire, a point where

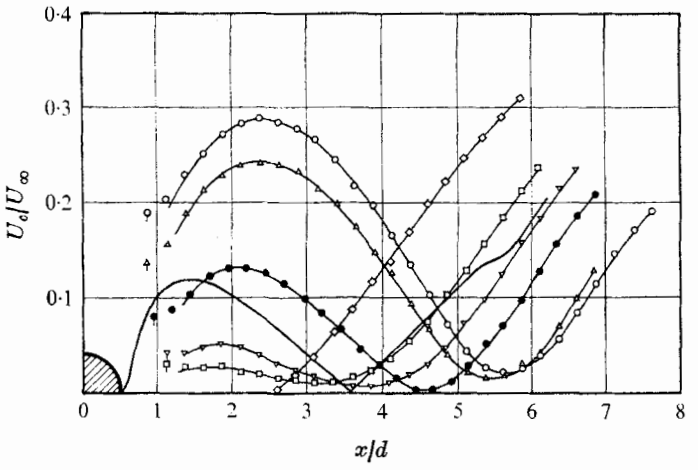

FIGURE 14. Velocity distributions along centre-line of wake. ◇, $R = 40$; □, $R = 55$; ▽, $R = 60$; ●, $R = 65$; △, $R = 75$; ○, $R = 80$. Flags on symbols indicate that the hot-wire reading was affected by the wall. ——, Takami & Keller's result at $R = 50$.

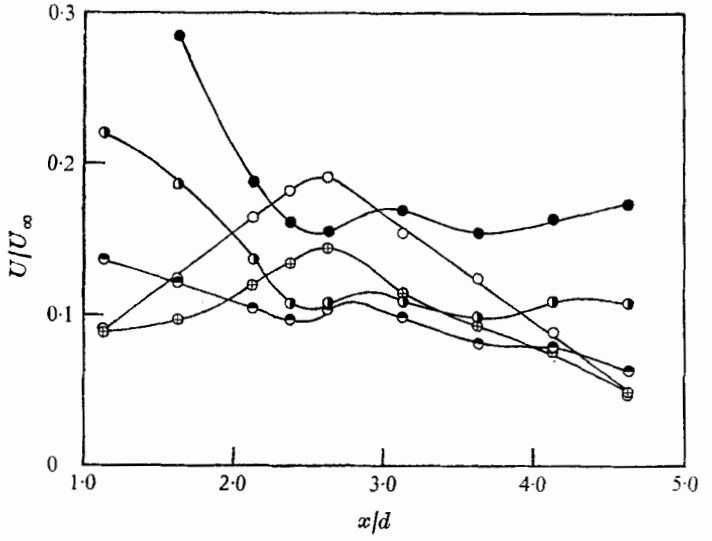

FIGURE 15. Velocity distributions along lines y/d = constant; $R = 80$. ○, $y/d = 0{\cdot}30$; ⊕, $y/d = 0{\cdot}375$; ◓, $y/d = 0{\cdot}45$; ◑, $y/d = 0{\cdot}525$; ●, $y/d = 0{\cdot}60$.

$U = 0$ does not appear in figure 15. The location of the valley may coincide with the centre of eddy. Peaks and valleys in figure 15 exist at the same x/d and the point of maximum U_c also coincides with the x position of the eddy centre.

According to the flow visualization experiments by Taneda (1956) the standing eddies appear at $R = 5$. In the present measurements the manifestation of the standing eddies, namely, the W-shaped distribution of U, is not found until R exceeds 60. This may not mean that there are no standing eddies for $R < 60$, but may mean that for $R < 60$ the scale of the eddies is too small to be resolved

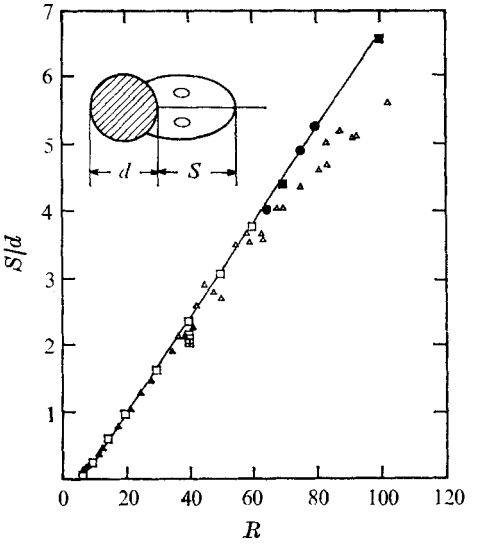

FIGURE 16. Length of standing eddies *vs.* Reynolds number. Experimental results: ●, present work; ▲, Taneda; △, Acrivos *et al.* Numerical solutions: □, Takami & Keller; ⊞, Kawaguti; ⊟, Apelt; ■, Dennis & Chang.

by the hot-wire anemometer. It is inevitable that the confined circulating flow inside standing eddies is slightly heated by the hot wire. This reduces the heat loss rate of the wire and consequently the anemometer indicates apparent velocities smaller than the true velocities. We tried to diminish the influence of the heating by operating the anemometer at various overheat ratios ranging from 0·15 to 0·6, but we found it impossible to get rid of the influence. Therefore, measurements made in the standing eddies for $R < 60$ may not be very accurate. However, the influence becomes smaller as the eddies become larger and the speed of the flow inside the eddies increases. Therefore, the measurements for $R > 60$ may be free from the heating effect. For this reason we discuss the structure of standing eddies mainly at $R = 65$, 75 and 80.

The wake stagnation point, which is the downstream end of the standing eddies, is determined from figure 14. The length S of the eddies is plotted against R in figure 16. Takami & Keller's and Dennis & Chang's numerical results lie on the straight line drawn through data of Taneda for small R and the present measurements for large R. The results of Acrivos *et al.* are slightly smaller than the present results for $R > 70$.

The maximum value U_{cc} of U_c increases with R and becomes as large as $0{\cdot}3U_\infty$ at $R = 80$ as shown in figure 14. The location x_c of the eddy centre moves downstream as R increases. Although decisive conclusions about the variation of U_{cc} and x_c with R are not obtained from the present measurements, x_c increases almost linearly with R for R between 55 and 75 and the value of x_c at $R = 50$, which is determined by the extrapolation of the linear relation down to $R = 50$, agrees well with the value of Takami & Keller.

On comparing the streamwise variation of U_c at $R = 65$ with that of the

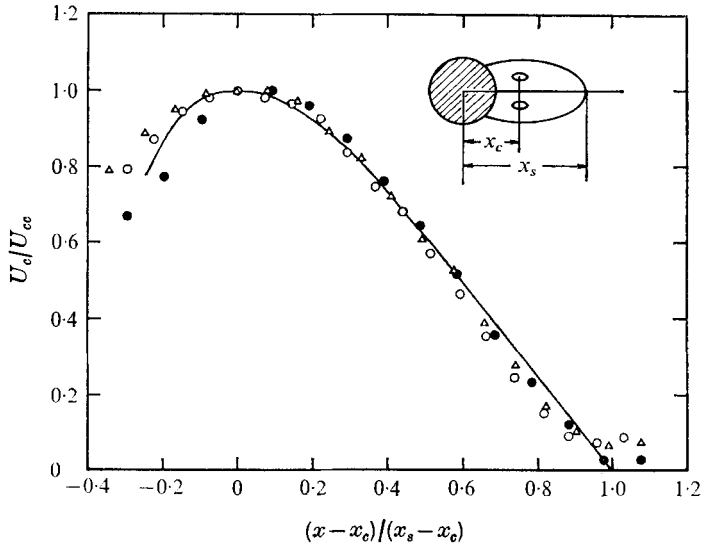

FIGURE 17. Non-dimensionalized velocity along the centre-line. ●, $R = 65$; △, $R = 75$; ○, $R = 80$; ——, Takami & Keller's numerical solution for $R = 50$.

numerical solution at $R = 50$ shown in figure 14, we notice that the two curves along the returning stagnation streamline are quite similar. In particular U_c varies almost linearly with x/d in the rear half of the eddies. This linear relation holds also at $R = 75$ and 80. These facts suggest the existence of similarity in standing eddies. In figure 17, U_c/U_{cc} is plotted against $(x-x_c)/(x_s-x_c)$, where x_s is the x co-ordinate of the wake stagnation point. It is seen that for

$$0 < (x-x_c)/(x_s-x_c) < 1$$

the experimental points at different Reynolds numbers collapse onto a single curve, which is very close to Takami & Keller's numerical result at $R = 50$. We conclude that the flow within the standing eddies is similar at Reynolds numbers from 65 to 80.

4. Conclusion

In this paper we have presented the results of measurements of the velocity distributions across the standing eddies as well as in the wake of a cylinder at Reynolds numbers from 10 to 80. Various existing numerical solutions have been compared with experimental results in detail. The following conclusions have been obtained.

(i) Takami & Keller's solutions agree with the experimental results at $R = 10$, but there are discrepancies at higher Reynolds numbers. The numerical results consistently deviate from the present results as x/d increases.

(ii) Imai's analytical formula for the far-field wake agrees quite well with the present measurements for $x/d > 10$ in the Reynolds number range 10–40.

(iii) The numerical results of Kawaguti and Apelt at $R = 40$ agree well with

the present experimental results for the drag coefficient and the length of the standing eddies but show considerable discrepancies in the development of the wake.

(iv) The velocity defect profiles for $R = 10$–40 are similar for $x/d > 10$.

(v) The length of the standing eddies grows linearly with R.

(vi) The velocity distribution along the returning stagnation streamline within the standing eddies has similarity.

The authors wish to express their cordial thanks to Professor S. Iida, University of Osaka Prefecture, for his support and helpful advice and to Dr H. Takami, University of Tokyo, for kindly providing the results of numerical solutions.

REFERENCES

Acrivos, A., Leal, L. G., Snowden, D. D. & Pan, F. 1968 *J. Fluid Mech.* **34**, 25.

Acrivos, A., Snowden, D. D., Grove, A. S. & Petersen, E. E. 1965 *J. Fluid Mech.* **21**, 737.

Apelt, C. J. 1961 *Aero. Res. Counc. R. & M.* no. 3175.

Collis, D. C. & Williams, M. J. 1959 *J. Fluid Mech.* **6**, 357.

Dennis, S. C. R. & Chang, G. Z. 1970 *J. Fluid Mech.* **42**, 471.

Grove, A. S., Shair, F. H., Petersen, E. E. & Acrivos, A. 1964 *J. Fluid Mech.* **19**, 60.

Imai, I. 1951 *Proc. Roy. Soc.* A **208**, 487.

Kawaguti, M. 1953 *J. Phys. Soc. Japan*, **8**, 747.

Keller, H. B. & Takami, H. 1966 *Numerical Solutions of Nonlinear Differential Equations* (ed. D. Greenspan), p. 115. Wiley.

Kovasznay, L. S. G. 1949 *Proc. Roy. Soc.* A **198**, 174.

Kovasznay, L. S. G. & Chevray, R. 1969 *Rev. Sci. Instrum.* **40**, 91.

Nishioka, M. 1972 *Bull. University of Osaka Prefecture*, **21**, 205.

Nishioka, M. 1973 *Bull. J.S.M.E.* **16**, 1887.

Nishioka, M. & Sato, H. 1970 *Bull. ISAS, University of Tokyo*, **6**, 571 (in Japanese).

Roshko, A. 1954 *N.A.C.A. Tech. Rep.* no. 1191.

Takami, H. & Keller, H. B. 1969 *Phys. Fluid Suppl.* II, **12**, II–51.

Taneda, S. 1956 *J. Phys. Soc. Japan*, **11**, 302.

Thom, A. 1933 *Proc. Roy. Soc.* A **141**, 651.

Tritton, D. J. 1959 *J. Fluid Mech.* **6**, 547.